



The influence of La-doping on the activity and stability of Cu/ZnO catalyst for the low-temperature water–gas shift reaction

Rothman Kam^a, Cordelia Selomulya^a, Rose Amal^b, Jason Scott^{b,*}

^a Department of Chemical Engineering, Clayton Campus, Monash University, Australia

^b ARC Centre of Excellence for Functional Nanomaterials, School of Chemical Sciences and Engineering, The University of New South Wales, Australia

ARTICLE INFO

Article history:

Received 22 February 2010

Revised 10 May 2010

Accepted 11 May 2010

Available online 8 June 2010

Keywords:

Water–gas shift

Cu/ZnO

Lanthanum

H₂O-TPD

CO-TPD

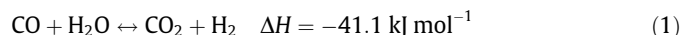
ABSTRACT

The influence of lanthanum (La) doping on the performance of 37 wt% Cu/ZnO catalysts for the low-temperature water–gas shift (LT-WGS) reaction was investigated. A 2.3 wt% La loading improved catalyst activity compared to the neat Cu/ZnO and Cu/ZnO/Al₂O₃ systems and was accompanied by a lowering of the activation energy. Higher La loadings promoted the adsorption of H₂O at the expense of CO, resulting in a decrease in LT-WGS activity. Additionally, 2.3 wt% La acted to stabilise catalyst activity compared with the neat Cu/ZnO. XPS and H₂-TPR assessment demonstrated a strong interaction between Cu and La components, while data from CO and H₂O-TPD studies favoured the associative WGS mechanism in this instance. Activity and stability findings also suggested metallic Cu was not responsible for LT-WGS activity.

© 2010 Elsevier Inc. All rights reserved.

1. Introduction

The water–gas shift (WGS) is a reversible, exothermic chemical reaction for conditioning product streams from the steam reforming of hydrocarbons for industrial hydrogen production. It describes the reaction between carbon monoxide and water vapour to produce carbon dioxide and hydrogen (Eq. (1)).



Commercially, the WGS reaction is performed in two stages to overcome the thermodynamic and kinetic limitations of the reaction. The two steps involve a high-temperature (350–500 °C) shift (HT-WGS) reaction typically over Fe₂O₃/Cr₂O₃ catalysts [1,2], at which the favourable kinetics can be exploited and the volume of the catalyst minimised, followed by a low-temperature (200–250 °C) shift (LT-WGS) reaction over a Cu/ZnO-based catalyst which takes advantage of the thermodynamic equilibrium at low temperature [1,3]. Currently, the LT-WGS typically requires a large reactor volume due to its slow reaction kinetics [1]. The LT-WGS has also been observed to occur in small reactors at low temperatures [4], although under these conditions the reverse reaction (i.e. CO generation) was favoured. Hence, it remains desirable to develop catalysts with higher activity to reduce steam production requirements [5], reduce the LT-WGS catalyst volume and ultimately reduce the costs associated with reactor size. Improving

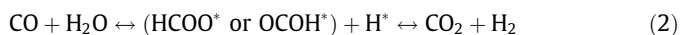
catalyst stability is also a major challenge for the Cu/ZnO system for LT-WGS reactions. It is well documented that Cu/ZnO is susceptible to sintering during reaction [6,7], resulting in a loss of active sites. Cu/ZnO deactivation has been reported to derive from carbonate build-up on the surface which acts as a reaction-inhibiting spectator specie [8].

Improved LT-WGS catalyst performance may be achieved by doping the Cu/ZnO with additional metal cations. This is the case for commercial Cu/ZnO/Al₂O₃ catalyst where alumina is employed to stabilise the ZnO and prolong catalyst life [1,2,5,9]. Alkaline-type cations have also been reported to improve Cu/ZnO LT-WGS activity. Shishido et al. [6] found doping Cu/ZnO with alkaline earth metals (Mg, Ca, Sr and Ba) increased catalyst activity but did not improve stability. Lanthanum (La) is an alkaline-type metal that has been demonstrated by Schaper et al. [10] to provide structural stability for a methanation catalyst support (γ-Al₂O₃).

Even though Cu/ZnO catalysts are well studied, uncertainties remain regarding the precise nature of the WGS mechanism. These mechanisms are generally believed to be either associative [11,12] or regenerative [6,13,14]. Salient features of the proposed WGS mechanisms involve the adsorption of CO and H₂O onto the catalyst surface [15]. Some hold the view that during the WGS reaction, a bifunctional synergistic effect exists between the copper and zinc oxide [16,17] where the copper species activates the CO molecule while the ZnO activates the water molecule [11,18]. The main difference between the two mechanisms concerns the formation of formate-type (HCOO⁻) and/or carboxyl-type (COOH⁻) intermediates that subsequently decompose into the reaction products (Eq. (2)) during the associative route [12,15,19].

* Corresponding author. Fax: +61 2 9385 5966.

E-mail address: jason.scott@unsw.edu.au (J. Scott).



The regenerative route consists of surface oxidation of a oxygen vacancy site (*) by water vapour (Eq. (3)) followed with surface reduction by carbon monoxide (Eq. (4)) [7,13].



The objective of this study is to explore the effect of lanthanum (La) as a promoter in the Cu/ZnO catalytic system during WGS reaction. In particular, the influence of La on Cu/ZnO catalyst activity and stability were investigated to gain greater insights into the mechanisms governing catalyst performance of La promoted Cu/ZnO catalyst. The catalysts were benchmarked against a commercial Cu/ZnO/Al₂O₃ formulation for the LT-WGS reaction.

2. Experimental

2.1. Catalyst preparation

A flame spray pyrolysis (FSP) reactor [20] was used to synthesise CuO, ZnO, Cu/ZnO, Cu/ZnO/La₂O₃ and Cu/ZnO/Al₂O₃ particles. In all cases, the Cu loading was maintained at approximately 37 wt%, while the Zn and La loadings were varied. The Cu/ZnO/Al₂O₃ catalyst (F-COM) was fabricated based on a typical commercial catalyst composition (weight ratio 37:55:8, respectively [21]). Precursor solutions containing predetermined amounts of metal oxides with a total molar concentration of 0.5 M were prepared by mixing zinc 2-ethylhexanoate (Alfa, purity > 99%), lanthanum (III) 2-ethylhexanoate (10 wt% in hexane solution, Aesar), aluminium s-butoxide (Strem, purity > 98%) and copper 2-ethylhexanoate (Aldrich, purity > 99.9%) in xylene (Riedel de Haen, 96%). During FSP synthesis, the liquid precursor was fed (rate: 5 ml min⁻¹) to the flame by a syringe pump (Inotech R232). The generated particles were collected on a glass fibre filter (Whatmann GF/D) with the aid of a vacuum pump (Alcatel). Detailed descriptions on other operating conditions can be found elsewhere [20]. La₂O₃ (Aldrich, 99.9%) was used as the La reference in this study.

2.2. Catalyst characterisation

X-ray diffraction (XRD) spectra were collected on a Philips X'Pert MPD instrument using Cu K α ($\lambda = 1.542 \text{ \AA}$) with scan range from 20° to 90° at a scan rate of 0.22° min⁻¹ and step size of 0.026°. Surface analysis of the catalysts was performed by X-ray photoelectron spectroscopy (XPS) on ESCALab220i-XL (VG Scientific) using a monochromatised Al K α radiation at a pass energy of 20 eV and at $P < 2 \times 10^{-9}$ mbar. The energy scale was calibrated and corrected for charging using the C1s (285.0 eV) line as the binding energy reference. Transmission electron microscope (TEM) imaging of the catalysts was performed using a Phillips CM-200 to observe size and morphology. Inductively coupled plasma optical emission spectrometry (ICP-OES) was used to determine the metal content in each synthesised sample. The measurements were taken on a Perkin-Elmer OPTIMA DV3000 apparatus, and the sample was dissolved in nitric acid (3 M) before measurement. Copper metal surface area (CSA) was determined by the N₂O decomposition method at 90 °C using the same experimental methodology reported by Jensen et al. [22], assuming a reaction stoichiometry of two Cu atoms per N₂ atom and a Cu surface density of 1.46×10^{19} atom m⁻² [23]. Prior to the measurement, 30 mg of sample was reduced at 230 °C for 30 min and flushed with He (50 ml min⁻¹) for a further 30 min. The specific surface areas (SSA) of the prepared catalysts were analysed by nitrogen adsorption at 77 K, on the Micromeritics Tristar 3000, using the BET model.

2.3. Temperature-programmed reduction, desorption and oxidation

Temperature-programmed reduction (TPR), H₂O and CO desorption (TPD) and oxidation (TPO) experiments were performed on a Micromeritics Autochem 2920 instrument interfaced with a thermal conductivity detector (TCD) with the results normalised to the mass of the sample used in the experiments. An isopropanol cooling trap was placed between the sample and the TCD to retain the water formed during the reduction process. Downstream to the TCD, gases were analysed with an online mass spectrometer (Balzers Thermostar Quadrupole). For TPR experiments, each sample (50 mg) was pre-treated at 120 °C under He (50 ml min⁻¹) for 1 h then cooled to ambient temperature. TPR was then performed under 5% H₂/He (50 ml min⁻¹) at a ramp rate of 5 °C min⁻¹ to 400 °C with the results recorded by the TCD.

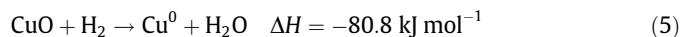
Before each H₂O-TPD experiment, the catalyst (50 mg) was reduced with 10% H₂/He (50 ml min⁻¹) at 230 °C for 1 h. The catalyst was then flushed for 1 h in He (50 ml min⁻¹) for the remainder of the TPD experiment. Deionised water (1.0 μL) was injected into the sample cell using a micro-syringe. Pulses were repeated five times with a 1-min interval between each injection, and the catalyst bed was then flushed with He for a further 30 min. Finally, the catalyst bed was ramped to 600 °C at a rate of 10 °C min⁻¹. The outlet gas was monitored by mass spectrometry (Balzers Thermostar) when H₂O was pulsed into the sample cell housing the reduced sample. No hydrogen was generated during this period.

During CO-TPD, the catalyst was reduced with 5% CO/He (50 ml min⁻¹) at 230 °C for 1 h followed by flushing under He (50 ml min⁻¹) for 1 h to remove physisorbed CO before returning to ambient temperature. The CO-TPD proceeded by ramping to 600 °C at a rate of 10 °C min⁻¹. In all TPD experiments, oxidative pre-treatment of catalysts to remove residue carbonaceous species derived during FSP synthesis was not employed. The temperature requirement to oxidize these species was too high (400–450 °C) [24] which would likely have invoked catalyst sintering and influenced the results.

During TPO, the catalyst bed was ramped to 500 °C at 10 °C min⁻¹ under 5% O₂/He (50 ml min⁻¹). No catalyst pre-treatment was conducted prior to TPO experiments.

2.4. Catalyst activity

Activity testing was performed using a 6 mm I.D. stainless steel packed bed reactor with the as-prepared catalyst sample (100 mg) diluted with α -Al₂O₃ (70 μm , 500 mg). Prior to each activity test, catalysts were reduced under a total flow of 100 ml min⁻¹ (10% H₂/N₂) for 1 h at 230 °C (ramp rate of 5 °C min⁻¹) and flushed with N₂ for 30 min before being returned to ambient temperature. The H₂ concentration and temperature ramping rate were selected to avoid thermal sintering of the catalyst due to the exothermic nature of the reduction from CuO to Cu metal reaction (Eq. (5)) [3].



The reactant gas stream typically comprised 7% CO, 8.5% CO₂, 23% H₂O, 37.5% H₂ and 25% N₂ (Coregas) at a flow rate of 100 ml min⁻¹ and was discharged at atmospheric pressure. Deionised water was added via a vapourizer fed by a high-precision syringe pump (ISCO Inst., model 260D). Operating temperatures ranged from 150 to 300 °C with 50 °C increments ramped at 10 °C min⁻¹. The product stream, after passage through an ice trap to remove water, was analysed using two gas chromatographs (Shimadzu GC8A) fitted with thermal conductivity detectors. One chromatograph was operated with helium as the carrier gas through a 1.8-m CTR I column (Alltech Associates, Inc) for CO₂, CO, N₂, O₂ and CH₄ analysis. The second chromatograph employed argon as the carrier gas through a

2-m molecular sieve 13X column (Alltech Associates, Inc.) for H₂ analysis. The CO conversion was far from thermodynamic equilibrium [25] due to design of the experimental set-up which induced low residence times to avoid mass transfer limitations on the results.

Catalyst stability was continuously evaluated at an operating temperature of 300 °C for 25 h. This temperature is higher than standard LT-WGS conditions (200–250 °C) [2,26] and was selected to accelerate the rate of any deactivation. Catalysts samples were not diluted with α -Al₂O₃ in this series of experiments due to the need for post-reaction characterisation. Further details regarding the calculations for CO conversion are provided in Supporting information (A).

3. Results

3.1. Structural properties of the catalysts

The XRD spectra of nominal 37 wt% Cu-loaded ZnO-based nanoparticles synthesised by FSP (Fig. 1) showed the hexagonal structure of ZnO [27] was maintained over the range of La-doping concentrations. The elevated Cu loading was also detectable by XRD and gave a weak Bragg reflection at $2\theta = 38^\circ$, belonging to the monoclinic CuO (1 1 1) phase [28]. There was no detectable XRD reflection from La₂O₃ crystallites and no shift in Bragg positions of ZnO with increasing La loading. Evaluation of the ZnO crystallite size from XRD using the Scherrer formula (Table 1) indicated Cu addition reduced the crystal size from 20 nm to 17 nm. The CuO (1 1 1) XRD reflection, indicated by (○) in Fig. 1, was too small for accurate crystallite size evaluation, hence CuO crystallite size could not be determined. Increasing La addition promoted further ZnO crystal size reduction to 13 nm at 11 wt% La. The decrease in crystallite size is reflected in the TEM images of neat, Cu-loaded and Cu/La-loaded ZnO (Fig. 2a–d). The TEM micrographs also indicated a shift in ZnO morphology moving from a rod-like shape for neat ZnO (Fig. 2a) to spherical particles upon Cu incorporation (Fig. 2b). Likewise, the decreasing crystal size influenced the specific surface areas of the neat and composite materials (Table 1) with a corresponding increase in this characteristic with increasing La loading. Although not depicted here, all the prepared samples exhibited Type II N₂ adsorption–desorption isotherms, suggesting

the particles are nonporous, as frequently observed for flame-made particles [29].

The bulk weight ratio of Cu, Zn and La determined by ICP-OES (Table 1) indicated actual cation loadings were close to the nominal values. Cu⁰ surface area increased from 7.6 m²/g for the neat material to 27.4 m²/g when mixed with Zn; however, the presence of La served to decrease the Cu⁰ surface area. This is reflected by a drop in the Cu metal dispersion from 12.4% for Cu/ZnO to between 5.4% and 8.4% depending on La loading (Table 1). A similar influence was observed when 8 wt% Al₂O₃ was included in the Cu/ZnO, with Cu dispersion decreasing from 12.4% to 3.9%.

3.2. XPS analysis

Changes to surface bonding with increasing La dopant concentration were monitored by measuring the binding energies (BE) of Cu 2p_{3/2}, Zn 2p_{3/2} and La 3d_{5/2} core electrons. BEs and surface atomic Cu/Zn and La/Cu ratios for La-doped Cu/ZnO catalysts are summarised in Table 2. Binding energy of O1s was not considered due to complications with the overlapping contribution of oxygen from CuO, La₂O₃ and the ZnO support.

The BEs of Cu 2p_{3/2} and Zn 2p_{3/2} gave values of 933.9 eV and 1020.9 eV, respectively, corresponding to CuO and ZnO (Table 2). These values differ slightly to those of Garbassi et al. [30] who reported values of 933.4 eV and 1022.2 eV, respectively. This may arise from the different synthesis routes during catalyst preparation as Garbassi and Petrini [30] used co-precipitation. The shift in BEs when comparing the neat ZnO, CuO and the composite material (Table 2) provides evidence of an interaction between the Cu²⁺ and Zn²⁺ species. The presence of Cu²⁺ species can be readily identified by a strong satellite peak at 944–945 eV [30,31] as seen in Fig. 3. This satellite peak implies copper species on the catalyst exist in the Cu²⁺ oxidation state following FSP synthesis [31]. The lack of a peak at 932 eV indicates negligible Cu⁰ or Cu⁺ is present on the catalyst surface [32]. Inclusion of La into the system shifted the Cu 2p_{3/2} peak maxima (Fig. 3) from 933.4 eV at low La loadings (1 wt%) to 933.7 eV at higher La loadings (11 wt%) and was accompanied by a decrease in La 3d_{5/2} peak maxima (Table 2) from 835.4 to 835.1 eV demonstrating an interaction between CuO and La₂O₃. The simultaneous and opposing changes to Cu 2p and La 3d BEs infer a decrease in electron density in the Cu nucleus by increasing La dopant concentration. La₂O₃ inclusion had no influence on the ZnO peak maxima.

The surface elemental ratios of Cu and Zn relative to La were estimated from intensity ratios normalised by an atomic sensitivity factor [33]. These ratios are listed in Table 2. It can be seen that the Cu/Zn ratios are lower than bulk ratios obtained from ICP analysis, indicating depletion in the Cu concentration on the particle surface. On comparing the La/Zn and La/Cu ratios, an opposite effect was observed, where the surface elemental ratio is higher than the bulk ratio.

3.3. TPR analysis

The TPR profile of pure FSP-prepared CuO (Fig. 4) shows a strong reduction peak at 290 °C which is assigned to the reduction of CuO to metallic Cu as described by Eq. (5). The lack of any additional peaks agrees with XPS results indicating no Cu⁺ species are present [34,35]. Peak shoulders appear for the composite material between 170 °C and 200 °C and are more pronounced for the 11.0 wt% La-doped and F-COM catalysts. Although bulk ZnO reduction is thermodynamically feasible, temperatures as high as 650 °C are required to reduce ZnO to metallic zinc [36] with no ZnO reduction peaks observed in this study (up to 400 °C). The Cu/ZnO composite material possesses a lower reduction temperature (~210 °C) than either of the neat materials, with this peak ascribed to CuO

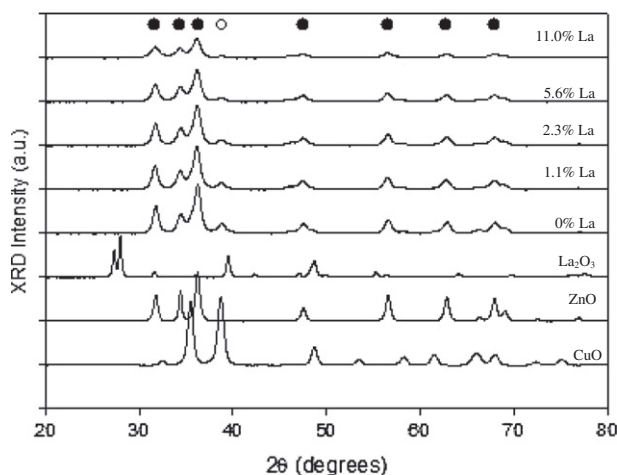


Fig. 1. XRD spectra (Cu K α , $\lambda = 1.542 \text{ \AA}$) of FSP-made nominal 37 wt% Cu/ZnO doped with varying La loadings. Pure CuO, ZnO and La₂O₃ are included for comparison. The solid circles (●) represent characteristic peaks of ZnO hexagonal wurzite-phase. The open circle (○) denotes peaks of monoclinic CuO (1 1 1) phase.

Table 1
Physicochemical properties, apparent activation energy and turnover frequency of neat, La-doped and Al-doped Cu/ZnO catalysts.

Catalyst (nominal weight ratio)	BET surface area ($\text{m}^2 \text{g}^{-1}$), SSA	Bulk composition in weight ratio ^a (mole ratio) (%)			Crystallite size ^b (nm)		Cu metal dispersion (%)	Cu surface area ^c ($\text{m}^2 \text{g}^{-1}$), CSA	E_a (kJ mol^{-1})	TOF ^d (s^{-1})
		Cu	Zn	La	d_{CuO}	d_{ZnO}				
CuO	35.8	100	0	0	25	–	1.4	7.6	–	–
ZnO	42.8	0	100	0	–	20	0	0	–	–
37% Cu/ZnO	67.5	37.3 (38.0)	62.7 (62.0)	0	–	17	12.4	27.4	42.9 ± 3	0.008
Cu/ZnO/La (37:62:1)	72.0	38.4 (39.3)	60.5 (60.2)	1.1 (0.5)	–	16	7.6	17.2	43.1	0.012
Cu/ZnO/La (37:61:2)	72.8	38.3 (39.4)	59.4 (59.5)	2.3 (1.1)	–	15	5.4	12.3	33.6	0.018
Cu/ZnO/La (37:58:6)	75.2	37.5 (39.7)	55.9 (57.6)	5.6 (2.7)	–	14	8.4	18.8	31.6	0.009
Cu/ZnO/La (37:50:11)	80.4	37.1 (40.1)	51.9 (54.5)	11.0 (5.4)	–	13	6.5	14.4	32.6	0.004
F-COM Cu/ZnO/Al ₂ O ₃ (37:55:8)	80.3	37.0 (38.8)	54.9 (55.9)	8.1 ^e (5.3)	–	14	3.9	8.6	60.9	0.063

^a Determined by ICP analysis.

^b Determined by XRD and Scherrer formula from averaging ZnO(1 0 0), ZnO(0 0 2) and ZnO(1 0 1) diffraction lines.

^c Determined by N₂O decomposition and the calculation of the copper surface area, it is assumed that a reduced copper surface has a surface density of 1.46×10^{19} copper atoms m^{-2} .

^d TOF for the overall WGS reaction on Cu/ZnO-based catalysts at 230 °C, 1 atm total pressure, 7% CO, 8.5% CO₂, 23% H₂O, 37.5% H₂ and 25% N₂.

^e Weight ratio of Al₂O₃ component.

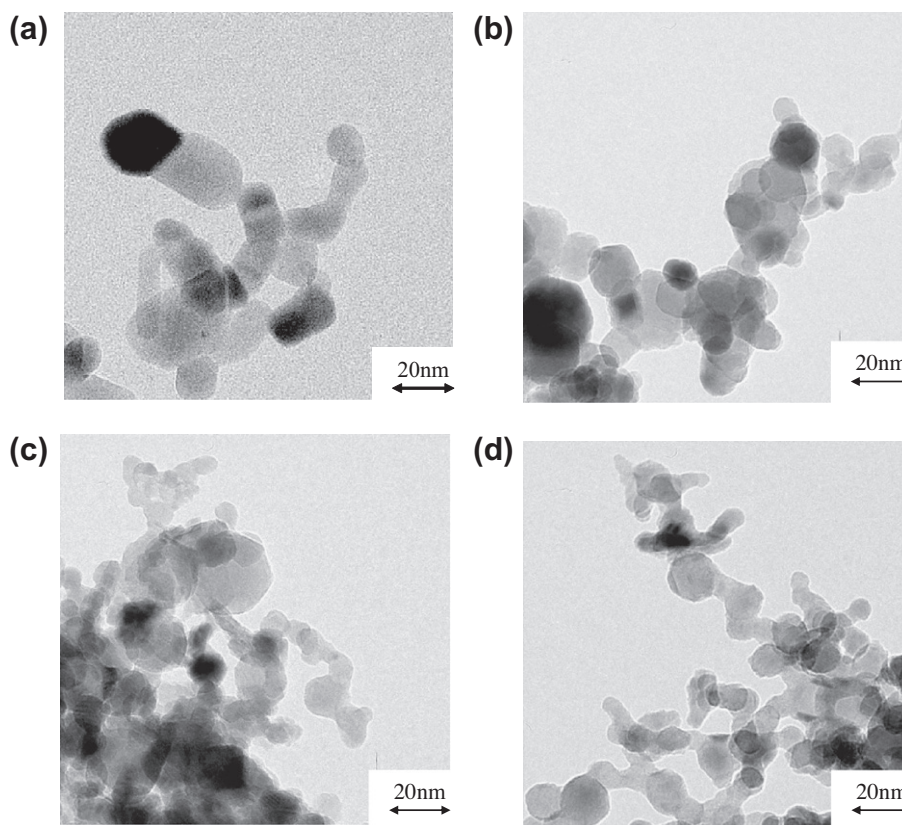


Fig. 2. TEM images of FSP-prepared (a) ZnO; (b) 37.3 wt% Cu/ZnO; (c) 5.6 wt% La-doped 37.5 wt% Cu/ZnO and (d) 11.0 wt% La-doped 37.1 wt% Cu/ZnO.

reduction and the temperature shift ascribed to interaction between the two oxides. The inclusion of La into the particles had minimal effect on the CuO reduction temperature up to a 2.3 wt% loading. Beyond this, La inclusion shifted the reduction temperature to higher values: 220 °C for 5.6 wt% and 230 °C for 11.0 wt%. The TPR profile of F-COM is included for reference and shows a reduction peak at ~ 235 °C.

3.4. TPD analysis

The TPD spectra of water adsorbed on the reduced catalysts are presented in Fig. 5. Water is strongly adsorbed on the neat FSP-ZnO surface as indicated by its gradual desorption from ~ 270 °C onwards, which accelerates at ~ 350 °C and culminates in a peak maxima at 420 °C. Similar chemisorption of H₂O on ZnO has been

Table 2
Binding energies of core electrons and XPS atomic ratios of as-prepared FSP catalysts.

Catalyst (nominal weight ratio)	XPS binding energies (eV)			Surface elemental ratio ^a (%)		
	Cu 2p _{3/2}	Zn 2p _{3/2}	La 3d _{5/2}	Cu/Zn	La/Zn	La/Cu
CuO	933.9	–	–	–	–	–
ZnO	–	1020.9	–	–	–	–
37% Cu/ZnO	933.4	1021.5	–	39.47 (61.29)	–	–
Cu/ZnO/La (37:62:1)	933.4	1021.5	835.4	49.98 (65.28)	1.42 (0.83)	2.79 (1.27)
Cu/ZnO/La (37:61:2)	933.5	1021.6	835.3	50.06 (66.22)	2.68 (1.85)	5.36 (2.79)
Cu/ZnO/La (37:58:6)	933.6	1021.5	835.2	51.78 (68.92)	6.50 (4.69)	12.54 (6.80)
Cu/ZnO/La (37:50:11)	933.7	1021.5	835.1	62.59 (73.58)	17.98 (9.91)	28.72 (13.47)

^a Values in parenthesis are elemental ratio determined by ICP analysis.

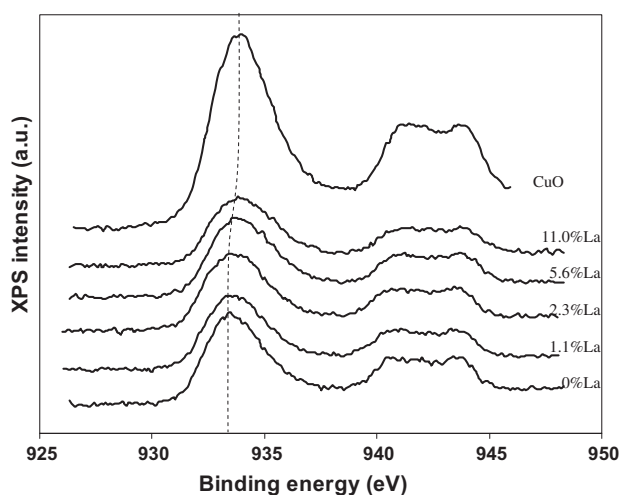


Fig. 3. Cu 2p_{3/2} XPS photoemission peak for FSP-prepared nominal 37% Cu/ZnO catalysts with varying La loadings. Pure FSP-prepared CuO is included for comparison.

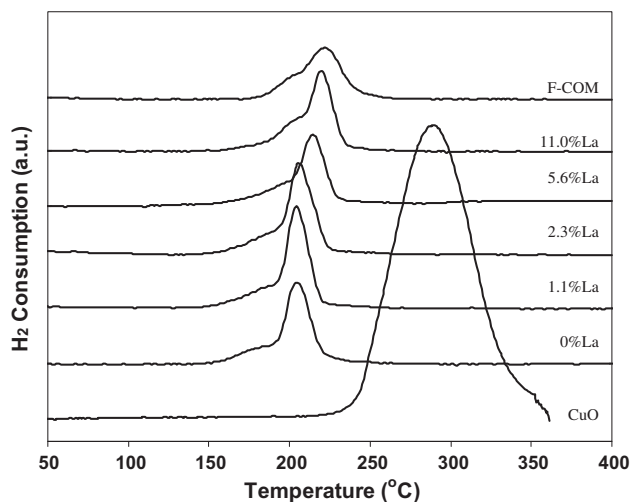


Fig. 4. H₂-TPR profiles of FSP-prepared 37% Cu/ZnO catalysts at different La dopant loading. Pure FSP-prepared CuO is included as a reference.

demonstrated by others [37,38]. Introducing Cu into the structure distinctly alters the H₂O-TPD profile with more rapid desorption beginning at ~270 °C, where it reaches a broader maxima between 370 and 400 °C, and then tapers off to around 600 °C. While La addition does not alter the general shape of the Cu/ZnO H₂O desorption profile, it does introduce some modifications. As the

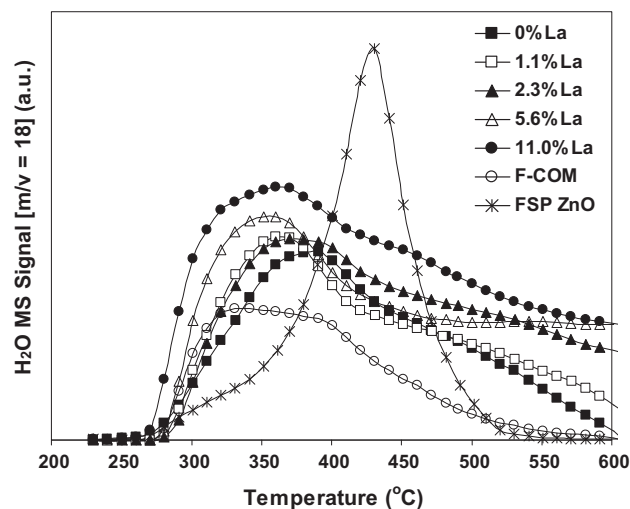


Fig. 5. H₂O-TPD profiles of FSP-prepared 37% Cu/ZnO catalysts with increasing La dopant loadings. F-COM represents the Al-doped catalyst and is included for comparison.

La loading is increased, the initial H₂O desorption front becomes steeper, the peak maxima increases and tapering off of the peak is slower (incomplete by 600 °C). In the case of F-COM, Fig. 5 indicates that while its desorption profile exhibits similarities to the Cu/ZnO profile, the presence of Al₂O₃ in a Cu/ZnO system does not facilitate H₂O adsorption, as demonstrated by the lower H₂O-TPD maxima. Reduced FSP-CuO was not observed to adsorb/desorb water (result not shown).

The findings demonstrate, while H₂O is strongly chemisorbed to ZnO, the inclusion of CuO has a substantial influence on the ZnO adsorption sites, shifting desorption to lower temperatures and broadening the desorption peak. Increasing La addition boosts H₂O desorption, encouraging greater desorption at the lower temperature and further broadening the adsorption site distribution.

The CO-TPD spectra on the reduced La/Cu/ZnO samples are shown in Fig. 6. Weakly chemisorbed CO was evident as small CO signals were detected at around 60–80 °C for all the samples which agrees with literature [39,40]. A dominant peak was also observed for all samples, exhibiting a maximum at between 300 °C and 320 °C. As the La loading increased, the amount of desorbed CO decreased and the peak maxima shifted to slightly higher temperatures. The presence of Al₂O₃ in the structure, as shown by the F-COM profile in Fig. 6 was detrimental to CO adsorption. CO-TPD on neat FSP-ZnO and reduced neat FSP-CuO did not show evidence of any CO adsorption (results not shown). Robert and Griffin studied a series of Cu/ZnO catalysts [39], prepared by different methods, using CO-TPD coupled with infrared (IR) spectroscopy. They found CO did not chemisorb on ZnO in their Cu-containing cata-

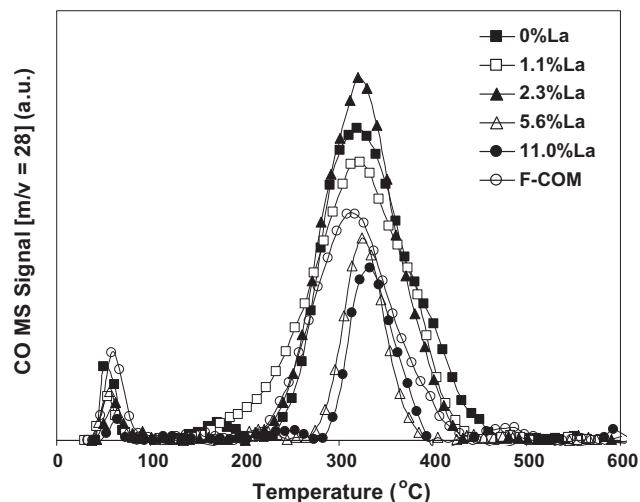


Fig. 6. CO-TPD profiles of FSP-prepared 37% Cu/ZnO catalysts at increasing La dopant loadings. F-COM represents the Al-doped catalyst and is included for comparison.

lysts but adsorbed only on the copper component [39]. To confirm the carbonaceous species deposited on the catalyst surface during FSP preparation did not influence CO-TPD results, the accompanying CO₂ signals are provided in Fig. S2 in the Supporting information (B).

3.5. WGS performance of catalysts

The effect of La content on the activity of FSP-prepared La/Cu/ZnO catalysts for the LT-WGS reaction is given in Fig. 7. While adding 1.1 wt% La had negligible influence on activity, promotion with 2.3 wt% La increased CO conversion by ~5% (to 44%) over the undoped Cu/ZnO catalyst. Further La addition was detrimental to LT-WGS activity with CO conversion dropping to ~50% (to 23%) of the undoped material for 5.6 wt% La loading. Apparent activation energies (*E_a*) were determined (Table 1) from the rates of CO consumption over the La/Cu/ZnO catalysts between 150 °C and 300 °C. The turnover frequencies (TOF) were also evaluated assuming the active sites were surface copper metal (Table 1).

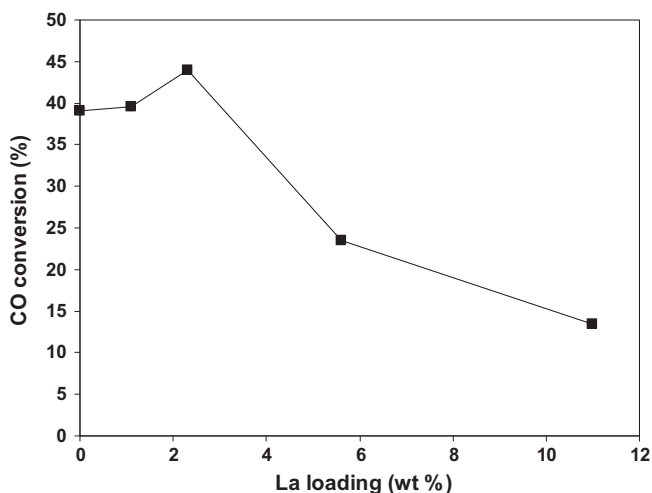


Fig. 7. Effect of lanthanum doping on CO conversion by 37 wt% Cu/ZnO (nominal) for the LT-WGS reaction. Reaction conditions: operating temperature = 300 °C, total flow = 100 mL min⁻¹ (7% CO, 8.5% CO₂, 23% H₂O, 37.5% H₂ and 25% N₂); catalyst loading = 0.10 g; pressure = 1 atm.

Cu/ZnO catalyst loaded with 2.3 wt% La invoked a substantial decrease in *E_a* (10 kJ mol⁻¹ difference), implying the forward WGS reaction was promoted. At greater La loadings, despite the decrease in CO conversion, the *E_a* remained relatively constant. No methane was detected in this study suggesting high selectivity of the Cu/ZnO catalysts. The stainless steel reactor did not contribute to LT-WGS activity in this study (see Fig. S3 in Supporting information (C)).

3.6. Catalyst stability and post-reaction characteristics

The stability of three catalyst samples: (i) 37.3 wt% Cu/ZnO; (ii) 2.3 wt% La-doped-38.3 wt% Cu/ZnO; and (iii) F-COM during the WGS reaction (at 300 °C) was assessed under 25 h of continuous run-time. CO conversion with operating time is shown in Fig. 8. Cu/ZnO conversion dropped by ~11% over the first 5 h after which it decreased a further 4% over the next 20 h. The presence of 2.3 wt% La markedly improved active site stability, although some deactivation was evident with an observed ~5% decrease in CO

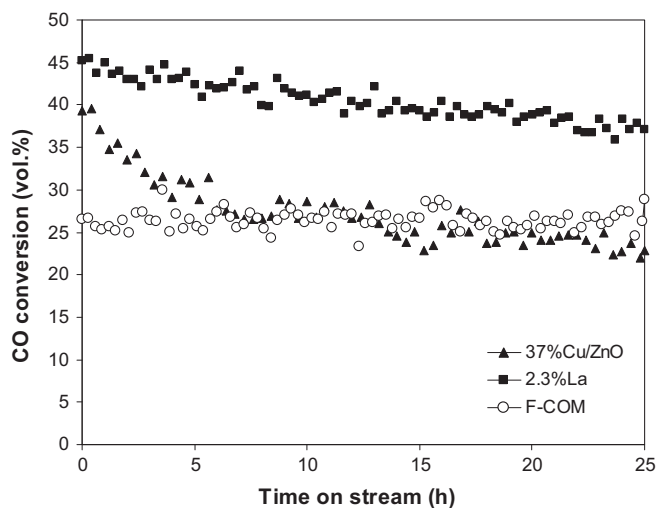


Fig. 8. CO conversion with time by 37.3% Cu/62.7% ZnO, 2.3% La/38.3% Cu/59.4% ZnO and F-COM (37% Cu/54.9% ZnO/8.1% Al₂O₃) for the LT-WGS reaction. Reaction conditions: temperature = 300 °C; flow rate = 100 mL min⁻¹ (7% CO, 8.5% CO₂, 23% H₂O, 37.5% H₂ and 25% N₂); catalyst loading = 0.10 g; pressure = 1 atm.

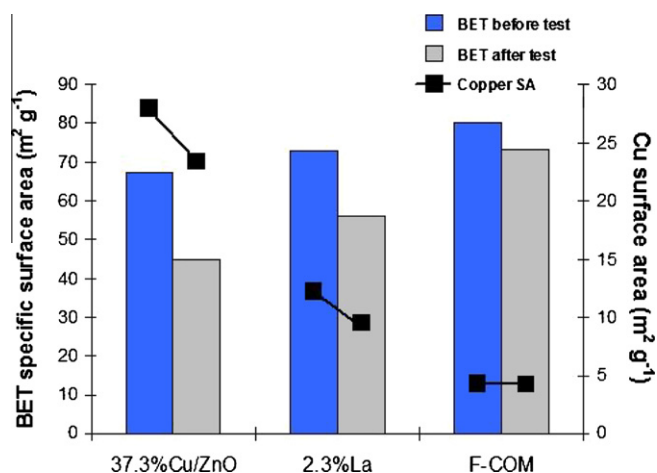


Fig. 9. Specific surface area and Cu surface area changes for 37.3% Cu/62.7% ZnO, 2.3% La/38.3% Cu/59.4% ZnO and F-COM (37% Cu/54.9% ZnO/8.1% Al₂O₃) following the LT-WGS reaction for 25 h. Reaction temperature = 300 °C.

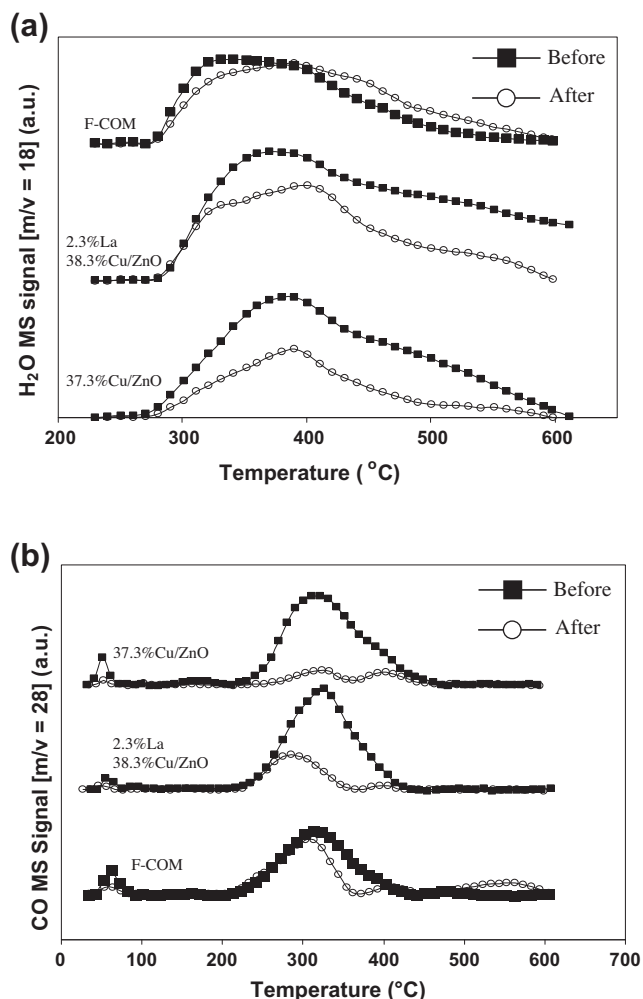


Fig. 10. Comparison of: (a) H₂O-TPD profiles and (b) CO-TPD profiles; for selected catalysts before and after 25 h LT-WGS reaction at 300 °C.

conversion over the 25-h period. Initial CO conversion by F-COM was approximately 15% and 20% lower than the undoped and La-doped catalysts, respectively; however, its activity was maintained over the 25-h time frame.

To aid in identifying the sources of catalyst deactivation/stability, surface areas (Fig. 9) and TPD profiles (Fig. 10) of the post-reaction materials were assessed. Fig. 9 indicates the Cu/ZnO catalyst lost 33% and 18% of its initial specific surface area (SSA) and copper surface area (CSA), respectively, during the reaction which may account for the activity loss incurred by this material. While La addition gave a mildly improved resistance to sintering (23% and 25% loss of its initial SSA and CSA, respectively) compared with the undoped Cu/ZnO, the loss of these attributes remained substantial but was not reflected by the catalyst activity. The presence of alumina in the catalyst make-up gave a lower initial activity but imparted increased stability for both the catalyst structure and the CSA. The 25-h reaction presented a small decrease in SSA (~8%), and negligible change in CSA. Fig. 9 also lends some support to the notion that Cu metal is not solely responsible for LT-WGS activity, as previously reported by Guo et al. [8]. Comparing the initial CSA's with initial LT-WGS activities indicates no correlation between the two.

Surface characterisation of the three post-reaction catalysts by H₂O-TPD and CO-TPD is shown in Fig. 10a and b, respectively. Fig. 10a indicates the 37.3%Cu/ZnO lost almost half its H₂O adsorption sites over the 25-h reaction period. The 2.3% La-loaded Cu/ZnO

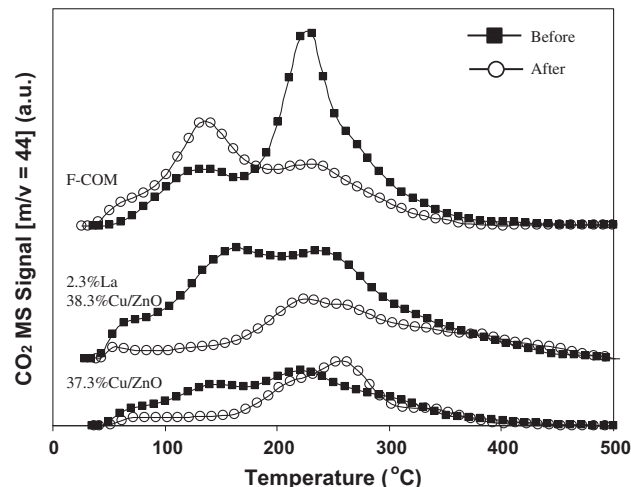


Fig. 11. Comparison of TPO curves for selected catalysts before and after the 25 h LT-WGS reaction at 300 °C.

catalyst also lost H₂O adsorption sites, however, to a lesser extent than the undoped material. In the case of F-COM, the loss of H₂O adsorption sites was small. Similar behaviour was observed for CO-TPD (Fig. 10b), with a substantial portion of the CO adsorption sites lost during reaction for the undoped and La-doped Cu/ZnO and a minor number lost for F-COM.

To assess whether a build-up of carbonaceous species contributed to catalyst deactivation, TPO experiments were conducted on the fresh and used catalysts. Fig. 11 shows no accumulation of carbonaceous species occurred on the catalyst surface during the LT-WGS reaction for the neat and La-doped Cu/ZnO system. In fact, it appears intrinsic carbonaceous species present on the fresh catalyst were removed during the WGS reaction as the CO₂ signal is generally lower for the used material. A strong CO₂ peak at 240 °C from the used-F-COM suggests a possible build-up of formates or carbonates occurs on the catalyst surface over the 25 h. Given there is no loss in activity for F-COM, it appears they behave only as spectator species.

4. Discussion

4.1. Structural and surface features of Cu/ZnO-based catalysts

Transition of the rod-shaped FSP-ZnO crystallites into smaller spherical ZnO crystals, as depicted in the TEM images (Fig. 2a and b), has been observed by others [41]. Zhu et al. [41] reported the morphology of nanostructured ZnO crystals could be altered by varying the growth temperature and Cu to Zn ratio. Cu plays an important role in confining the lateral growth of ZnO due to competition between Zn and Cu for oxygen [41] which may be evident in the oxidative combustion process during FSP synthesis [42]. Increasing La or Al-dopant loading effectively decreased the Zn content in the catalyst bulk and had the effect of increasing the Cu loading relative to Zn. This is expected to induce enhanced competition for oxygen by the Cu during synthesis and may be the source of the increasingly smaller ZnO crystallite sizes as demonstrated by XRD (Table 1) and TEM (Fig. 2a–d).

The decrease in metallic Cu surface area with increasing La loading may arise from the formation of a solid solution between CuO and La₂O₃ crystals. Jacobs and Jayadevan derived a phase diagram for the Cu–La–O system at 930 °C [43] and indicated a solubility limit of 40 mol% CuO in La₂O₃ can be achieved without altering the La₂O₃ structure.

Intensification of the TPR profile shoulder (Fig. 4) as La loading was increased in the Cu/ZnO system may be due to a reduction in surface CuO that is kinetically faster and precedes bulk CuO reduction [35]. The shoulder is significant for the 11.0 wt% La-doped and F-COM catalysts possibly due to their high specific surface areas (80.4 and 80.3 m²/g, respectively). That is, the particles possess a lower average size which in turn can affect the kinetics of surface CuO reduction [35].

Pestryakov and Davydov [44] used CO adsorption with IR spectroscopy to show the surface basicity of La₂O₃ to be very high due to the strong charge density on La₂O₃ oxygen ions. They were able to observe an electron donor–acceptor interaction between Cu^{x+} ions and La₂O₃ which indicated a loss of electron density in the Cu²⁺ nucleus due to electron scavenging properties of the La₂O₃. We observed from XPS a diminishing electron density in the Cu²⁺ nucleus manifested as a gradual shift in the Cu 2p_{3/2} spectra (Table 2) to higher binding energies (Fig. 3), with increasing La loading. This agrees well with Pestryakov and Davydov's work [44]. The decreasing Cu²⁺ electron density implies the Cu²⁺ and O²⁻ bond is strengthened by La addition as the Cu²⁺ becomes more positively charged. This is reflected in the H₂-TPR profiles with the gradual shift in reduction peaks from 205 to 225 °C for 2.3–11 wt% La/Cu/ZnO (Fig. 4) where the oxygen has become increasingly harder to remove from CuO.

The lower Cu/Zn surface ratio from XPS analysis compared with the bulk ratios acquired from ICP implies the CuO is not uniformly distributed throughout the ZnO matrix. The homogeneous solubility limit of Cu in ZnO has been reported as 10 mol% [45] which is considerably lower than the Cu loading used in this FSP catalyst. This alludes to the idea that CuO may exist (in part) as inclusions within the ZnO particles. Additionally, similar transition temperatures from vapour to liquid phase at atmospheric pressure for CuO at 2000 °C [46] and vapour to solid phase at 1900 °C for ZnO [47] may induce component segregation during the FSP formation process. In the case of La ratio with respect to Cu and Zn, the XPS surface elemental ratio is consistently higher than the bulk ratio (Table 2), suggesting an enrichment of La on the catalyst surface due to nucleation of the La₂O₃ component after CuO and ZnO during synthesis.

4.2. Catalytic behaviour, active sites and mechanism

The activity results (Fig. 7) demonstrated a decrease in CO conversion for La loadings greater than 2.3 wt%. This coincided with the shift to higher CuO reduction temperatures at La loadings greater than 2.3 wt% during TPR. The shift may be explained by the XPS findings which indicated increasing La addition decreased Cu core electron density, making it more difficult to remove O from the surface CuO. Coupled with this, CO-TPD results (Fig. 6) showed La loadings of 5.6 wt% and above promoted a significant loss in CO adsorption capacity of the catalyst. The loss in CO adsorption capacity may derive from the increase in La loading on the surface (with increasing La content) blocking surface active sites or electronic changes it may invoke on the adsorption sites. Given the Cu component of the catalyst is reported to be responsible for CO adsorption [39], it appears that increasing the La content beyond 2.3 wt% has a detrimental influence on both its electronic properties and capacity for adsorbing CO, in turn promoting the observed loss in catalyst activity.

Table 1 demonstrated that La addition decreased Cu metal dispersion by between 6.5% and 12.4% over the neat Cu/ZnO. Relating this finding to the activity results in Fig. 7 indicates no apparent correlation between the two, implying this characteristic is not responsible for LT-WGS catalyst activity. This notion is supported by the changing TOF values provided in Table 1, whereby if the surface Cu metal was responsible for the LT-WGS activity then the TOF

would remain constant over all the Cu/ZnO-based catalysts. This finding suggests Cu species other than metallic Cu may be responsible for the LT-WGS activity. Cu has been reported by Okamoto et al. [48] to coexist in various oxidation states on the Cu/ZnO catalyst surface. Using XPS on reduced Cu/ZnO, they revealed for high copper content catalysts (>25 wt% CuO), the predominant Cu metal species was well-dispersed metallic copper (Cu⁰) with Cu⁺ species also present, originating from CuO dissolved in the ZnO lattice. More recently, Harikumar and Rao [49] confirmed the existence of Cu⁰ and Cu⁺ species on their reduced Cu/ZnO using Auger spectroscopy analysis. Additionally, surface Cu⁺ has a high affinity to bind with CO molecules [49–53]. For instance, Didziulis et al. [54] conducted extensive work on heats of adsorption of CO on different well-defined copper sites and on the ZnO surface. They associated a high affinity of CO binding site with Cu⁺ centres on ZnO(0 0 0 1) and ZnO(1 0 1 0) dimers [54].

H₂O-TPD studies (Fig. 5) indicated the ZnO substrate was responsible for adsorbing water, although Cu addition substantially altered the H₂O desorption profile of the support, shifting the peak maxima to a lower temperature. La addition appeared to generally increase the amount of H₂O bound to the catalyst surface compared with neat Cu/ZnO. Lanthanum oxide is known to be highly hygroscopic [55], forming lanthanum hydroxide when exposed to water vapour and then desorbing water under thermal treatment (370 °C), to return to its oxide form (Eq. (6)) [56].



Notably, increasing La content increased the amount of H₂O desorbed between 280 °C and 400 °C. This temperature range overlays the CO desorption temperature range and suggests La may increase the amount of H₂O adsorbed at the expense of CO, particularly at loadings greater than 2.3 wt%.

Overall, the TPD results imply the ZnO substrate is primarily responsible for adsorbing the H₂O molecules, although the addition of Cu to the system lowers the strength by which they are bound to the surface. Cu on the other hand appears responsible for CO adsorption, although this does not derive from its metallic state but some other species, possibly Cu⁺. This site bifunctionality rules in favour of the associative mechanism during LT-WGS. That is, following H₂O and CO adsorption on the catalyst surface, carbonaceous intermediates are formed which then decompose into the desired products, CO₂ and H₂ [11,57,58].

The inclusion of La into the catalyst promotes a mild improvement in activity at 2.3 wt% after which higher loadings are detrimental to catalyst performance. The higher activity at 2.3 wt% is reflected in the lower activation energy at this loading (compared with 1.1 wt% La and neat Cu/ZnO), while further increases in La loading appear to promote H₂O adsorption at the expense of CO. This may provide the source of the observed lower activities. Liu and Rodriguez [59] concluded that dissociation of water is the rate-limiting step in a Cu catalytic system for WGS reaction. Hence, the presence of La increases the water adsorption and provides an initial decrease in activation energy for the water dissociation.

4.3. Catalyst stability and deactivation

It is well documented that Cu/ZnO is susceptible to sintering [6,7] during WGS operation, with a small amount of refractory oxide such as Al₂O₃ or Cr₂O₃ typically added to stabilise the Cu/ZnO structure, post-reaction catalyst characterisation showed two effects were evident. First (with the exception of the Al-loaded system), there were losses in catalyst surface area and Cu surface area, the extent depending on the additive. Secondly, there was a loss in CO and H₂O adsorption capacity for the neat and La-loaded catalysts but not for the Al-loaded system. The loss in substrate and Cu surface areas for the neat Cu/ZnO may account for the ob-

served decrease in LT-WGS activity with time; however, this is not the case for the La-loaded system with comparative losses in these two characteristics not emulated by the activity decrease. This implies the La acts to preserve the active sites despite the occurrence of thermal sintering. Thermal sintering does appear to govern the relative losses in CO and H₂O adsorption capacity of the catalysts, although the extent of loss in adsorption capacity is not closely correlated with the activity results. These findings also succinctly demonstrate the capacity of Al for stabilising the Cu/ZnO structure, albeit at the expense of activity.

TPO characterisation indicated deactivation did not result from the build-up of carbonaceous species. F-COM was the only catalyst to show carbonaceous species formed and remained on the surface during reaction but there was no corresponding activity decrease. This agrees with the findings by Guo et al. who reported a similar build-up of carbonate species on their Cu/ZnO/Al₂O₃ catalyst; however, they suggested the presence of these species on the catalyst surface, rather than sintering, coincided with deactivation [8].

5. Conclusions

La addition has been demonstrated to affect the activity and stability of Cu/ZnO catalysts under realistic feed conditions for the LT-WGS reaction. In particular, doping with 2.3 wt% La decreased the apparent activation energy of the Cu/ZnO system and improved the WGS activity compared to undoped Cu/ZnO. Further increase in La loading appears to promote H₂O adsorption at the expense of CO. This may provide the source of the observed lower activities. Moreover, the La stabilised the active sites over an extended operating period with the rate of deactivation markedly decreased despite a substantial decrease in specific and metallic copper surface area during reaction. These results implied metallic copper sites were not responsible for the LT-WGS activity. XPS characterisation revealed electron interaction between Cu and La components which corroborates the increase in Cu²⁺ binding energy to O²⁻ from increased concentration of La dopant. This is reflected by the increasing temperature required to reduce the CuO to metallic copper. The CO and H₂O-TPD studies imply the WGS mechanism proceeds via an associative route in the La-doped Cu/ZnO catalytic system.

In comparison with the Cu/ZnO/Al₂O₃ system, the La-doped Cu/ZnO is superior in terms of WGS activity even though a loss in activity is apparent over 25 h of WGS operation at 300 °C.

Acknowledgments

The authors acknowledge Dr. Bill Bing Gong and Katie Levick of the University of New South Wales for their assistance in collecting and interpreting XPS spectra and TEM images, respectively. The author is grateful for Dr. Wey Yang Teoh for his assistance during FSP synthesis.

Appendix A. Supplementary material

Supplementary data associated with this article can be found, in the online version, at [doi:10.1016/j.jcat.2010.05.004](https://doi.org/10.1016/j.jcat.2010.05.004).

References

[1] W. Vielstich, A. Lamm, H.A. Gasteiger, Catalyst development for water-gas shift, in: J.R. Ladebeck, J.P. Wagner (Eds.), *Handbook of Fuel Cells – Fundamentals, Technology and Applications*, vol. 3, John Wiley & Sons, Chichester, UK, 2003, p. 190.

[2] C.H. Bartholomew, R.J. Farrauto, *Fundamentals of Industrial Catalytic Processes*, John Wiley & Sons, Ltd., Hoboken, NJ, 2006.

[3] C. Rhodes, G.J. Hutchings, A.M. Ward, *Catal. Today* 23 (1995) 43–58.

[4] E. Bogel-Lukasik, R. Bogel-Lukasik, M.N.d. Ponte, *Monatsh. Chem.* 140 (2009) 1361–1369.

[5] D.S. Newsome, *Catal. Rev. Sci. Eng.* 21 (1980) 275–318.

[6] T. Shishido, M. Yamamoto, I. Atake, D. Li, Y. Tian, H. Morioka, M. Hondac, T. Sano, K. Takehira, *J. Mol. Catal. A: Chem.* 253 (2006) 270–278.

[7] T. Shishido, M. Yamamoto, D. Li, Y. Tian, H. Morioka, M. Honda, T. Sano, K. Takehira, *Appl. Catal. A* 303 (2006) 62–71.

[8] P.-J. Guo, L.-F. Chen, G.-B. Yu, Y. Zhu, M.-H. Qiao, H.-L. Xu, K.-N. Fan, *Catal. Commun.* 10 (2009) 1252–1256.

[9] M.S. Spencer, *Top. Catal.* 8 (1999) 259–266.

[10] H. Schaper, E.B.M. Doesburg, L.L.v. Reije, *Appl. Catal.* 7 (1983) 211–220.

[11] T. Shido, Y. Iwasawa, *J. Catal.* 129 (1991) 343–355.

[12] D.C. Grenoble, M.M. Estadt, D.F. Ollis, *J. Catal.* 67 (1981) 90–102.

[13] N.A. Koryabkina, A.A. Phatak, W.F. Ruettinger, R.J. Farrauto, F.H. Ribeiro, *J. Catal.* 217 (2003) 233–239.

[14] G.C. Chinchén, M.S. Spencer, K.C. Waught, D.A. Whan, *J. Chem. Soc. Faraday Trans.* 183 (1987) 2193–2212.

[15] J.L.C. Fajin, M.N.D.S. Cordeiro, Francesc Illas, J.R.B. Gomes, *J. Catal.* 268 (2009) 131–141.

[16] R. Burch, R.J. Chappell, S.E. Golunski, *Catal. Lett.* 1 (1988) 439–444.

[17] Y. Okamoto, K. Fukino, T. Imanaka, S. Teranishi, *Chem. Lett.* (1984) 71–74.

[18] G. Ghiotti, F. Bocuzzi, *Catal. Rev. Sci. Eng.* 29 (1987) 151–182.

[19] T.v. Herwijnen, W.A.D. Jon, *J. Catal.* 63 (1980) 83–93.

[20] W.Y. Teoh, L. Mädlar, D. Beydoun, S.E. Pratsinis, R. Amal, *Chem. Eng. Sci.* 60 (2005) 5852–5861.

[21] M.J.L. Gines, N. Amadeo, M. Laborde, C.R. Apesteguia, *Appl. Catal. A* 131 (1995) 283–296.

[22] J.R. Jensen, T. Johannessen, H. Livbjerg, *Appl. Catal. A* 266 (2004) 117–122.

[23] J.W. Evans, M.S. Wainwright, A.J. Bridgewater, D.J. Young, *Appl. Catal.* 7 (1983) 75–83.

[24] X. Liu, W. Ruettinger, X. Xu, R. Farrauto, *Appl. Catal. B* 56 (2005) 69–75.

[25] G.C. Chinchén, P.J. Denny, J.R. Jennings, M.S. Spencer, K.C. Waugh, *Appl. Catal.* 36 (1988) 1–65.

[26] J.R. Ladebeck, J.P. Wagner, *Handbook of Fuel Cells – Fundamentals, Technology and Applications*, Part 2 3 (2003) 190–201.

[27] G. Shen, J.H. Cho, J.K. Yoo, G.-C. Yi, C.J. Lee, *J. Phys. Chem. B* 109 (2005) 5491–5496.

[28] W. Wang, Y. Zhan, G. Wang, *Chem. Commun.* (2001) 727–728.

[29] S.E. Pratsinis, *Prog. Energy Combust. Sci.* 24 (1998) 197–219.

[30] F. Garbassi, G. Petrini, *J. Catal.* 90 (1984) 106–112.

[31] C.C. Chusuei, M.A. Brookshier, D.W. Goodman, *Langmuir* 15 (1999) 2806–2808.

[32] W.-L. Dai, Q. Sun, J.-F. Deng, D. Wu, Y.-H. Sun, *Appl. Surf. Sci.* 177 (2001) 172–179.

[33] M. Daturi, C. Binet, J.-C. Lavalley, A. Galtayries, R. Sporkenb, *PCCP* 1 (1999) 5717–5724.

[34] F. Nishida, I. Atake, D. Li, T. Shishido, Y. Oumi, T. Sano, K. Takehira, *Appl. Catal. A* 337 (2008) 48–57.

[35] M. Turco, G. Bagnasco, U. Costantino, F. Marmottini, T. Montanari, G. Ramis, G. Busca, *J. Catal.* 228 (2004) 43–55.

[36] T. Imoto, Y. Harano, Y. Nishi, S. Masuda, *Bull. Chem. Soc. Jpn.* 37 (1964) 441–444.

[37] C. Zwicker, K. Jacobi, *Surf. Sci.* 131 (1983) 179–194.

[38] R. Zhang, A. Ludviksson, C.T. Campbell, *Surf. Sci.* 289 (1993) 1–9.

[39] D.L. Roberts, G.L. Griffin, *J. Catal.* 110 (1988) 117–126.

[40] J. Strunk, R.N. d'Alnoncourt, M. Bergmann, S. Litvinov, X. Xia, O. Hinrichsen, M. Muhler, *PCCP* 8 (2006) 1556–1565.

[41] Y. Zhu, C.-H. Sow, T. Yu, Q. Zhao, P. Li, Z. Shen, D. Yu, J.T.-L. Thong, *Adv. Funct. Mater.* 16 (2006) 2415–2422.

[42] R. Strobel, A. Baiker, S.E. Pratsinis, *Adv. Powder Technol.* 17 (2006) 457–480.

[43] K.T. Jacob, K.P. Jayadevan, *J. Mater. Sci.* 37 (2002) 1611–1620.

[44] A.N. Pestryakov, A.A. Davydov, *Appl. Surf. Sci.* 103 (1996) 379–483.

[45] S.V. Ketchik, T.P. Minyukova, L.L. Kuznetsova, L.M. Plyasova, T.M. Yurieva, G.K. Borekov, *React. Kinet. Catal. Lett.* 19 (1982) 345–349.

[46] E. Mack, G.G. Osterhof, H.M. Kraner, *JACS* 45 (1922) 617–623.

[47] D.F. Anthrop, A.W. Searcy, *J. Phys. Chem.* 68 (1964) 2335–2342.

[48] Y. Okamoto, K. Fukino, T. Imanaka, S. Teranishi, *J. Phys. Chem.* 87 (1983) 3747.

[49] K.R. Harikumar, C.N.R. Rao, *Appl. Surf. Sci.* 125 (1998) 245–249.

[50] E.I. Solomon, P.M. Jones, J.A. May, *Chem. Rev.* 93 (1993) 2623–2644.

[51] D.F. Cox, K.H. Schulz, *Surf. Sci.* 249 (1991) 138–148.

[52] G.E. Parris, K. Klier, *J. Catal.* 97 (1986) 374–384.

[53] K.-D. Jung, O.-S. Joo, *Bull. Korean Chem. Soc.* 23 (2002) 1765–1768.

[54] S.V. Didziulis, K.D. Butcher, S.L. Cohen, E.I. Solomon, *JACS* 111 (1989) 7110–7123.

[55] J. Kwon, M. Dai, M.D. Halls, E. Langereis, Y.J. Chabal, R.G. Gordon, *J. Phys. Chem. C* 113 (2009) 654–660.

[56] A. Neumann, D. Walter, *Thermochim. Acta* 445 (2006) 200–204.

[57] T. Shido, Y. Iwasawa, *J. Catal.* 140 (1993) 575–584.

[58] Y. Amenomiya, G. Pleizier, *J. Catal.* 76 (1982) 345–353.

[59] P. Liu, J.A. Rodriguez, *J. Phys. Chem.* 1226 (2007) 164705.